Characterization of High-Density Flowing Plasmas Using a Directional Micro-Retarding Potential Analyzer

IEPC-2005-170

Presented at the 29th International Electric Propulsion Conference, Princeton University, October 31 – November 4, 2005

James Partridge and Nikolaos A. Gatsonis
Worcester Polytechnic Institute, Worcester, MA 01609, U.S.A.

Abstract: A Retarding Potential Analyzer (RPA) consists of a series of variably biased electrodes allowing ions with sufficient energy access to a collection plate while repelling electrons and other low energy ions. The dimensions of the RPA, including electrode spacing and orifice diameter, are inversely restricted to the density of the incident plasma, making high-density measurements of ion energy distributions susceptible to space charge limited inaccuracies. A 200 μm diameter single-orifice or single-channel RPA has been coupled with a Microchannel Plate (MCP) of 0.326% transparency to relax these constraints, producing viable ion energy measurements within plasma plumes of number density greater than $1x10^{18}$ m^{-3}. To calculate the expected ion current measured by the RPA current collection plate for a given range of plasma properties, a triple numeric integration scheme was applied. Using nested numeric integration methods for each integral with functionally dependent upper bounds, the resultant Current Collection Theory (CCT) accounts for both geometric flux limitations as well as voltage sweeping effects similar to that of a classical gridded RPA. This paper focuses on the analysis of I-V curve sample data, specifically the determination of ion parameters using the developed CCTs for each type of RPA design. While nonlinear least squares regression was applied to provide a reliable calculation of ion drift velocity, ion temperature, and ion number density using both the classical RPA CCT as well as the Multi-Channel micro-Retarding Potential Analyzer (MC-μRPA) CCT, iterative methods were required when using the Single-Channel micro-Retarding Potential Analyzer (SC-μRPA) CCT.

Nomenclature

A	=	area
a, b, c, d	=	finite integral bounds
$\mathbf{C}(\mathbf{r}, t)$	=	peculiar velocity vector
$\mathbf{c}(\mathbf{r}, t)$	=	total velocity vector
$\mathbf{c}_0(\mathbf{r}, t)$	=	mean velocity vector
C	=	peculiar speed
c	=	total speed
c_0	=	mean speed
d	=	diameter
$d^3\mathrm{v}$	=	volume of velocity space element
E_{eff}	=	effective energy corresponding to ϕ_{eff}
ES_n	=	Simpson's rule approximation error
f	=	distribution function
f^4	=	integrand's fourth derivative
g_1, g_2	=	upper bound function values
I, I_{cp}	=	collector plate current
$Inner$	=	pertaining to the innermost integral
k	=	Boltzmann constant
L	=	collision length
l	=	length
m	=	mass
M_4	=	integrand's fourth derivative maximum
$Middle$	=	pertaining to the middle integral
$Outer$	=	pertaining to the outermost integral

*Graduate Research Assistant, Department of Mechanical Engineering, jimmyp@wpi.edu.
† Professor, Department of Mechanical Engineering, gatsonis@wpi.edu.

$\hat{n}$ = unit normal vector
$n(\mathbf{r},t)$ = number density
$N_{cc}(S,D)$ = number flux without wall collisions
$N_{cr}(S,X)$ = number flux with wall collisions
$\dot{N}_s$ = number flux of species s
Q = fluxal quantity
q = charge
$\mathbf{r}$ = position vector
r = radius
S = ion speed ratio
$\vec{S}$ = ion speed ratio vector
s = pertaining to species s
T = temperature
t = time
V = effective potential ratio
v_{eff} = effective velocity corresponding to ϕ_{eff}
$w(X,D)$ = Clausing probability function
X = normalized channel length
Y = arbitrary integration variable
β = inverse of most probable ion velocity
$\chi(S)$ = Patterson flux component
χ_{MCP} = MCP transmission fraction
$\Delta y, \Delta z$ = step sizes
ϕ = effective potential, azimuthal angle
ϕ_{eff} = effective retarding potential
φ = cylindrical flux integration angle
$\eta(S,D)$ = Patterson flux component
λ_D = Debye length
θ = elevation angle
$\vec{\Xi}$ = total velocity ratio vector
$\vec{\Psi}$ = peculiar velocity ratio vector
$\Psi(D)$ = Patterson flux component
ζ = arbitrary integration angle
$\{u,v,w\}$ = total velocity components
$\{u_0,v_0,w_0\}$ = drift velocity components
$\{U,V,W\}$ = peculiar velocity components
$\{\hat{u},\hat{v},\hat{w}\}$ = velocity space unit normal vectors
$\{\hat{\mathrm{x}},\hat{\mathrm{y}},\hat{\mathrm{z}}\}$ = Cartesian unit normal vectors

I. Introduction

THOROUGH characterization of ions and neutrals is one of the most important issues in the design and optimization process of many electric propulsion devices and plasma sources. Energy analyzers have been utilized for decades in both ground-based experiments and *in situ* diagnostics packages for the analysis of electric propulsion thrusters, atmospheric plasmas, plasma processing, and other plasma flow applications. Retarding Potential Analyzers (RPAs) are particularly useful in this process, as they are capable of characterizing both ion and neutral parameters. RPAs systematically filtrate the electrons and low energy ion species of an incident plasma through the use of a series of electrically biased grids or electrodes. Only ions of a sufficient energy level and neutrals have access to a collector plate. An RPA generally consists of four to five electrodes: A Floating Electrode (FE) grounded to the external plane of the RPA housing provides an electrically uniform environment to the incident plasma. An Electron Retarding Electrode (ERE) is biased negatively to repel all incident electrons. One to two Ion Retarding Electrodes (IREs) are used to repel low energy ions (Two IREs are used to prevent degradation of the desired electric field.).[1] Finally, a Secondary Electron Suppression Electrode (SESE) is used to prevent any low energy electrons emitted due to secondary emission or specific ionization from traveling to the collector plate.[2] I-V curves are generated by taking ion current measurements at various IRE potentials, allowing for the determination of ion number density, ion temperature, and ion drift velocity.[3] Neutral densities can be determined by biasing the IREs to repel all ions, allowing only the neutrals to be counted by a particle collector.[4]

RPAs can be categorized under three basic design types: traditional gridded RPAs, spherical RPAs, and single-orifice (or single-channel) RPAs. Gridded RPAs are generally used for relatively low-density plasmas, have been used for electric propulsion device characterization in both ground-based experiments and *in situ* diagnostics packages. For example, a traditional gridded RPA was implemented to study the ion species found in the Charging Hazards and Wake Studies (CHAWS) experiment, which encountered ion number densities no greater than $1\text{x}10^{12}$ m^{-3}.[5] The Spherical RPAs, which are similar to gridded RPAs in that they have a series of concentric spherical grids, have been used to characterize the ionosphere on Space Shuttle flights STS-3/OSS-1 and STS-51/SL-2.[6] Of particular interest for high-density plumes (greater than $1\text{x}10^{18}$ m^{-3}) is the single-channel RPA design due to the constraints employed to avoid space charge limitations within the RPA electrode series.[7] Space charge effects will not only increase the likelihood for substrate breakdown, arcing, or other electrical breakdown phenomena, but will also decrease the accuracy of the RPA.[8] The Debye length (λ_D) is the virtual limit of space charge neutrality, and it is necessary to restrict the single orifice diameter to no more than two Debye lengths, and the spacing of electrodes to no more than four Debye lengths.[9] Conversely, sizing the RPA too small will result in a weak ion current signal

strength. This can be solved by increasing the Debye length of the plasma incident to the RPA by means of a low transparency mesh or entrance slit.[10] Figure 1 shows the measurement capability of a single-channel RPA as it adheres to the orifice diameter constraint (assumes an electron temperature of 10 eV).

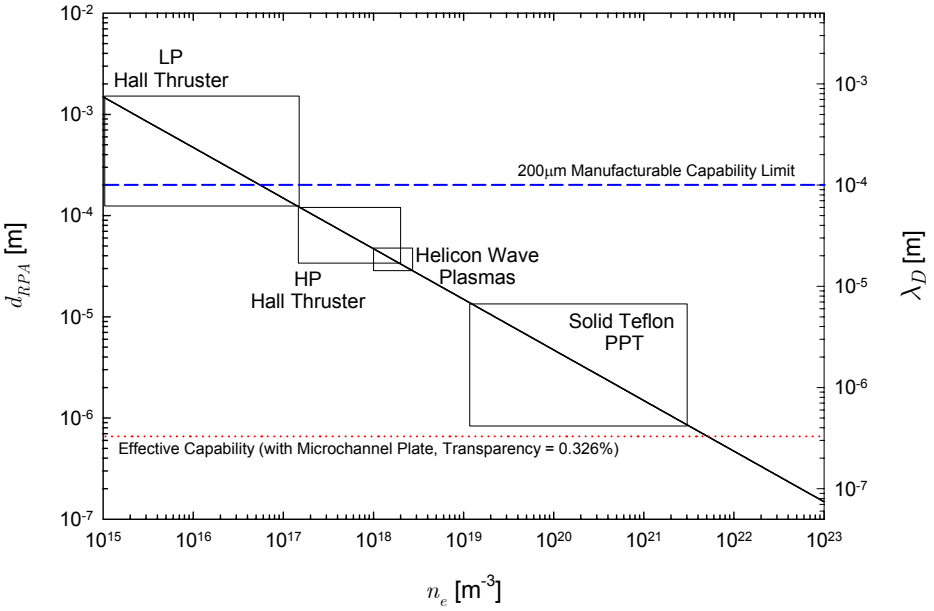

Figure 1. RPA capabilities and optimum RPA orifice diameter as a function of number density.

A low transparency Microchannel Plate (MCP) was combined with a Single-Channel micro-RPA (SC-μRPA) to relax the λ_D constraint, as shown in Figure 2. The resultant Multi-Channel micro-RPA (MC-μRPA) design increases the diagnostic's capability to perform accurate measurements of Pulsed Plasma Thrusters (PPTs), high-powered Hall thrusters, and other high-density plumes.[11]

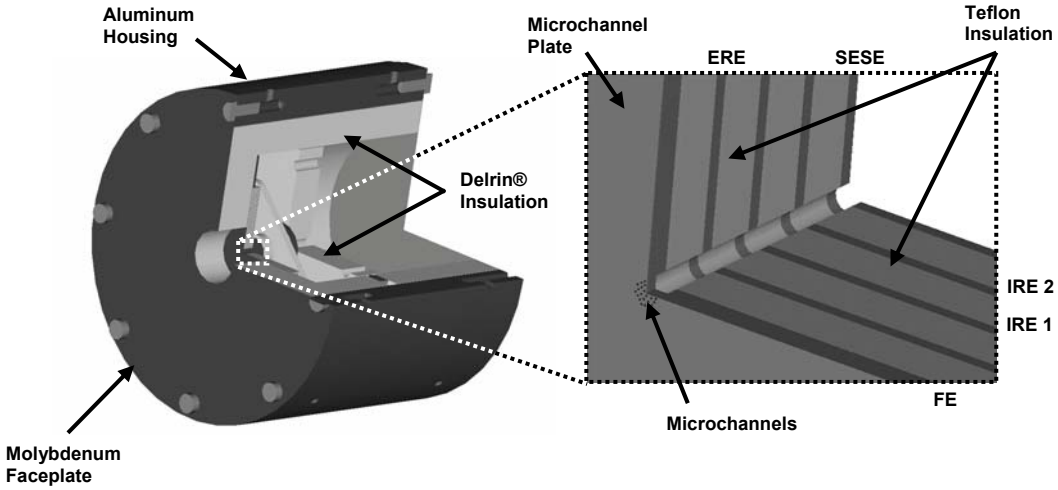

Figure 2. MC-μRPA housing, insulation, and aperture.

The complexity of the resultant design hinders the development of any proper analytical model for eventual use in the device's Current Collection Theory (CCT). Classical expressions require numeric integration so that nonlinear

least squares regression and current derivative methods can no longer be applied to determine macroscopic ion properties.

II. DμRPA and Single Orifice Current Collection Theory

To develop an analytical model which accounts for both cylindrical channel flux limitations and voltage sweeping effects, it is first necessary to derive the less complex cases, specifically the surface number flux of a drifting Maxwellian plasma through an electrically biased surface element and the number flux limitation through a cylindrical channel, derived in spherical coordinates.

The μRPA Current Collection Theory (CCT) can then be modeled as the combination of a cylindrical channel (of MCP geometry) with an electrically biased exit surface. The Single-Channel micro-RPA (SC-μRPA) is then modeled as a cylindrical channel at a constant effective retarding potential. All drifting plasma species are assumed to be Maxwellian. The expressions concern only positively charged ion species and all potentials are assumed to be positive.

A. Velocity Descriptions

The linear velocity of a molecule measured at its center of mass as it moves with respect to a given reference frame of Cartesian unit vector axes $\{\hat{x},\hat{y},\hat{z}\}$ can be denoted as the vector $\mathbf{c}(\mathbf{r},t)$, indicating a dependence on both position and time. The molecular speed, c, is defined by the magnitude of $\mathbf{c}(\mathbf{r},t)$. This total velocity vector would then have components $\{u,v,w\}$ corresponding to a position vector in a velocity space of unit vector axes $\{\hat{u},\hat{v},\hat{w}\}$. Triple integration over components u,v,w would then correspond to a volume integral in velocity space, allowing for calculation of velocity distributions and other fluxal properties.[12]

While individual molecules each have total velocity $\mathbf{c}(\mathbf{r},t)$ relative to a given reference frame, a flow comprising of a single-species gas has a macroscopic velocity relative to that same reference frame. Weighted by molecular mass, this macroscopic velocity is called the mean mass velocity, or mean velocity, and at any point $\mathbf{r},t$ is given by

$$\mathbf{c}_0(\mathbf{r},t) = \frac{\sum \mathbf{c}(\mathbf{r},t)}{n(\mathbf{r},t)d\mathbf{r}} \tag{1}$$

having components $\{u_0,v_0,w_0\}$. The summation over $\mathbf{c}(\mathbf{r},t)$ is performed over $nd\mathbf{r}$ molecules.[12] Similarly, $n(\mathbf{r},t)$ and $c(\mathbf{r},t)$ are averaged over a small time interval from t to $t+dt$. The mean speed is then defined by

$$c_0 = \frac{\sum c}{nd\mathbf{r}}. \tag{2}$$

While the notation can be dropped as shown above, mean speed is also dependent upon $\mathbf{r}$ and t.

With the mean mass velocity defined, there exists a molecular velocity measured in relation to a reference frame moving at mean mass velocity. This is known as the peculiar velocity, $\mathbf{C}(\mathbf{r},t)$, having components $\{U,V,W\}$. By definition

$$\mathbf{C}(\mathbf{r},t) = \mathbf{c}(\mathbf{r},t) - \mathbf{c}_0(\mathbf{r},t). \tag{3}$$

The velocity vector diagram can be seen in Figure 3.

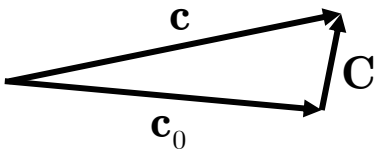

Figure 3. Velocity vector diagram.

Therefore, the total velocity of a molecule is the sum of the molecule's peculiar velocity and the mean velocity of the entire flow.[12] The peculiar speed of a molecule is denoted by C.

B. Surface Number Flux for a Maxwellian Drifting Plasma with an Applied Potential

The flux of some quantity Q having number density n and total velocity vector $\mathbf{c}$ $\{u, v, w\}$ through a surface element in the negative $\hat{n}$ direction is given by $n\overline{Qu}$, assuming that $\hat{n} = \hat{\mathrm{x}}$ and that $\mathbf{c}$ lies within the x-y plane.[12] The surface element coordinate system is shown in Figure 4, where the total velocity vector consists of both a mean velocity, $\mathbf{c}_0$ $\{u_0, v_0, w_0\}$, and a peculiar velocity vector, $\mathbf{C}$ $\{U, V, W\}$, such that $\mathbf{c} = \mathbf{C} + \mathbf{c}_0$. In Cartesian coordinates, the fluxal quantity $n\overline{Qu}$ can be rewritten by incorporating the distribution function, to obtain

$$n\overline{Qu} = n\int_{-\infty}^{\infty}\int_{-\infty}^{\infty}\int_{0}^{\infty} Qufdudvdw \tag{4}$$

where f is the distribution function.[13] Assuming a Maxwellian distribution for a mixed equilibrium gas with a mean velocity $\mathbf{c}_0 = 0$, the distribution function f for any single species s can then be expressed as

$$f = \frac{\beta^3}{\pi^{3/2}}\exp(-\beta^2 C_s^2) \tag{5}$$

where

$$\beta = \left(\frac{m_s}{2kT}\right)^{1/2}. \tag{6}$$

To determine the inward normal flux for a single species s in equilibrium through a surface element, the quantity Q is set equal to 1. Expanding the integrals containing the distribution, with $\mathbf{c} = \mathbf{C}$, gives the following expression:

$$\dot{N}_s = \frac{n_s\beta^3}{\pi^{3/2}}\int_{-\infty}^{\infty}\exp(-\beta^2 W_s^2)dW_s\int_{-\infty}^{\infty}\exp(-\beta^2 V_s^2)dV_s\int_{0}^{\infty}U_s\exp(-\beta^2 U_s^2)dU_s\,. \tag{7}$$

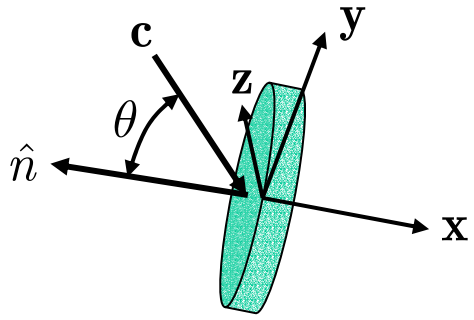

Figure 4. Molecular flux across a surface element.

To develop an identical expression in spherical coordinates using the distribution function, it is necessary to express the volume of velocity space element in the form of

$$d^3\mathrm{v} = c^2\sin\theta d\theta d\phi dc \tag{8}$$

where c is the total particle speed, θ is the polar angle, and ϕ is the azimuth angle. Since the number of particles striking the surface element per unit time is $(c\cos\theta)fd^3\mathrm{v}$, the distribution of speeds can then be expressed for a single species s as

$$\dot{N}_s = \frac{n_s\beta^3}{\pi^{3/2}}\int_0^{\infty}\int_0^{\pi/2}\int_0^{2\pi} c_s\cos\theta\exp(-\beta^2 C_s^2)c_s^2\sin\theta d\phi d\theta dc_s\,. \tag{9}$$

Further simplification occurs with the substitution of total speed ratio $\Xi = \beta c_s$, and since the total velocity $\mathbf{c}$ is the same as the peculiar velocity $\mathbf{C}$ in this case, the distribution of speeds can be rewritten as

$$\dot{N}_s = \frac{n_s}{\beta\pi^{3/2}}\int_0^{\infty}\int_0^{\pi/2}\int_0^{2\pi}\Xi^3\cos\theta\exp(-\Xi^2)\sin\theta d\phi d\theta d\Xi\,. \tag{10}$$

If the surface element has an effective potential resultant from an applied potential close to the element, a portion of the positively charged particles within the stationary gas will be repelled. If the effective potential ϕ_{eff} of

the surface element corresponds to an effective energy E_{eff} and an effective velocity v_{eff}, then the inward flux will only consist of molecules having velocity greater than v_{eff}. This effective potential is taken into account by modifying the lower bound of the x-direction velocity integral of the inward number flux expression. A spherical coordinate system derivation requires a modification of the lower bound of total speed integration. Since this bound is dependent on θ, this integral must be performed prior to the elevation angle integral:

$$\dot{N}_s = \frac{n_s}{\beta\pi^{3/2}} \int_0^{\pi/2} \int_{V_{eff}/\cos\theta}^{\infty} \int_0^{2\pi} \Xi^3 \cos\theta \exp(-\Xi^2) \sin\theta d\phi d\Xi d\theta \,. \tag{11}$$

A drifting plasma having a mean velocity vector $\mathbf{c}_0$ would make some angle θ with the surface element normal vector $\hat{n}$. Assuming θ lies entirely in the x-y plane, then a molecule's total velocity components would be comprised as follows:

$$\begin{aligned} x&: \quad \mathrm{u} = U + u_0 = U + c_0 \cos\theta \\ y&: \quad \mathrm{v} = V + v_0 = V + c_0 \sin\theta \\ z&: \quad \mathrm{w} = W \end{aligned} \tag{12}$$

which indicates that particles having x-direction peculiar velocity greater than $-c_0 \cos\theta$ will pass through the surface element. To calculate inward normal flux in a spherical coordinate system for a drifting gas, vector analysis of velocities is required to manipulate the distribution of speeds. In this case, the total velocity vector $\vec{\Xi}$ is not equal to the peculiar velocity vector $\vec{\Psi}$, where $\Psi = \beta C_s$. Instead, $\vec{\Psi} = \vec{\Xi} - \vec{S}$, as shown in Figure 5. $\vec{S}$ is the mean velocity vector, where $S = \beta c_{0s}$.[14]

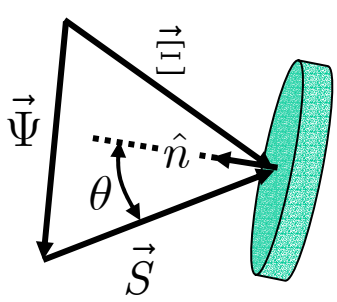

$$\vec{\Xi} = \vec{\Psi} + \vec{S}$$
$$\vec{\Xi} = \beta \mathbf{c}_s$$
$$\vec{\Psi} = \beta \mathbf{C}_s$$
$$\vec{S} = \beta \mathbf{c}_{0s}$$

Figure 5. Velocity ratio vector diagram with surface element.

The distribution of speeds is then written as

$$\dot{N}_s = \frac{n_s}{\beta\pi^{3/2}} \int_0^{\infty} \int_0^{\pi/2} \int_0^{2\pi} \Xi^3 \cos\theta \exp(-\Psi^2) \sin\theta d\phi d\theta d\Xi \,. \tag{13}$$

It is then necessary to obtain an expression for Ψ^2 in terms of Ξ. From Figure 5,

$$\Psi^2 = \Xi^2 + S^2 - 2\left|\vec{\Xi}\right|\left|\vec{S}\right|\cos\theta \tag{14}$$

which leads to

$$\dot{N}_s = \frac{n_s}{\beta\pi^{3/2}} \int_0^{\infty} \int_0^{\pi/2} \int_0^{2\pi} \Xi^3 \cos\theta \exp(-(\Xi^2 + S^2 - 2\left|\vec{\Xi}\right|\left|\vec{S}\right|\cos\theta)) \sin\theta d\phi d\theta d\Xi \,. \tag{15}$$

Assuming the drift velocity is aligned with the surface element normal vector and taking into account the effects of both an applied potential and a drift velocity, integration along the x-direction peculiar velocity from $v_{eff} - c_{0s}$ to infinity, is shown by

$$\dot{N}_s = \frac{n_s \beta^3}{\pi^{3/2}} \int_{-\infty}^{\infty} \exp(-\beta^2 W_s^2) dW_s \int_{-\infty}^{\infty} \exp(-\beta^2 V_s^2) dV_s \int_{v_{eff}-c_{0s}}^{\infty} (U_s + c_{0s}) \exp(-\beta^2 U_s^2) dU_s \,. \tag{16}$$

Integration yields

$$\dot{N}_s = \frac{n_s}{2\pi^{1/2}}\left[\frac{\exp(-\beta^2(v_{eff}-c_{0s})^2)}{\beta} + c_{0s}\sqrt{\pi}\{1-\mathrm{erf}(\beta(v_{eff}-c_{0s}))\}\right]. \tag{17}$$

When converted to current and taking into account area, this expression is known as the classical RPA CCT, as shown by

$$I_{RPA} = q\dot{N}_s A = \frac{qn_s A}{2\pi^{1/2}}\left[\frac{\exp(-\beta^2(v_{eff}-c_{0s})^2)}{\beta} + c_{0s}\sqrt{\pi}\{1-\mathrm{erf}(\beta(v_{eff}-c_{0s}))\}\right]. \tag{18}$$

To obtain the classical RPA current collection theory through a spherical coordinate system derivation, it is necessary to combine the effects that drift and applied potential have on the distribution of speeds. Specifically, the lower bound of the speed integral must be modified, elevation angle θ integration must be performed last, and the Ψ^2 identity must be applied. These requirements result in the following distribution of speeds:

$$\dot{N}_s = \frac{n_s}{\beta\pi^{3/2}}\int_0^{\pi/2}\int_{Veff/\cos\theta}^{\infty}\int_0^{2\pi}\Xi^3\cos\theta\exp(-(\Xi^2+S^2-2\left|\vec{\Xi}\right|\left|\vec{S}\right|\cos\theta))\sin\theta d\phi d\Xi d\theta\ . \tag{19}$$

Integrating first with respect to ϕ and then with respect to Ξ yields

$$\begin{aligned}\dot{N}_s = \frac{n_s}{2\beta\pi^{1/2}}\int_0^{\pi/2}\tan(\theta)\exp\left[-\left(\frac{V^2}{\cos^2\theta}+S^2(1+\sin^2\theta)\right)\right]\bullet \\ \left\{2\exp\left[2SV+S^2\sin^2\theta\right](V^2+\cos^2\theta+SV\cos^2\theta+S^2\cos^4\theta)\right. \\ +S\pi^{1/2}\cos^3(\theta)\exp\left[\frac{V^2}{\cos^2\theta}+S^2\right]\left[3+2S^2\cos^2\theta+2S^2\cos^2(\theta)erf\left(\frac{-V+S\cos^2\theta}{\cos\theta}\right)\right. \\ \left.\left.+3erf\left(\frac{-V+S\cos^2\theta}{\cos\theta}\right)\right]\right\}d\theta.\end{aligned} \tag{20}$$

This expression contains eight terms, the last two of which contain the error function of a cosine as shown. When integration over θ is performed using a standard symbolic integration kernel such as Maple[15] or Mathematica[16], all but the last two terms will properly integrate. The precise problem exists in the error function of a cosine. Numerical integration is required, and for all cases, values match that of the classical RPA CCT derived in Cartesian coordinates.

C. Cylindrical Channel Flux Limitations

In a cylindrical channel of diameter to length ratio D, the flux of neutral particles can be classified into two species: those which travel through the entire channel without collision with the inner wall and those which have at least one collision with the inner wall. Particles within the latter species are classified by the location of their first collision with the inner wall at a normalized axial location between X and $X+dX$. The total flux of particles through a cylindrical tube can then be expressed by

$$N = N_{cc}(S,D) + \int_0^1 N_{cr}(S,X)w(X,D)dX \tag{21}$$

where N_{cc} is the uninhibited flux, and N_{cr} is the flux containing particle/wall collisions, as shown in Figure 6. The $w(X,D)$ term is the emergence probability function of particles exiting the channel based on diffuse reflection. Due to the introduction of potentials along the channel's inner wall, one can assume 100% wall absorption. Through this assumption, the total flux is equal to the uninhibited flux.

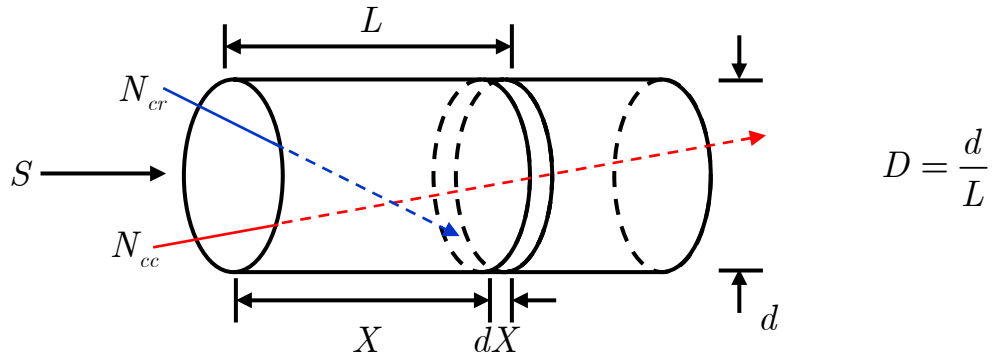

Figure 6. Number flux species through a cylindrical channel of finite diameter to length ratio, D.

There are at least two known methods of calculating the uninhibited flux of neutral particles. While both methods operate in a spherical regime and produce the same results, only one method, developed by Patterson (1971), manipulates the distribution function in spherical coordinates using vector analysis.[14] Patterson's expression is as follows:

$$N_{cc}(S,D) = \frac{nC_m}{2\sqrt{\pi}}\pi r^2\left[\chi(S) - \Psi(D)\exp(-S^2) - \frac{4S}{\sqrt{\pi}}\eta(S,D)\right] \tag{22}$$

with

$$\chi(S) = \exp(-S^2) + S\sqrt{\pi}(1+erf(S))\,, \tag{23}$$

$$\Psi(D) = \frac{2}{D^2}\left(\sqrt{1+D^2}-1\right), \text{ and} \tag{24}$$

$$\eta(S,D) = \frac{1}{D}\int_0^1 dY \int_0^{\tan^{-1}D\sqrt{1-Y^2}} [1+erf(S\cos\varphi)]\cos\varphi\exp(-S^2\sin^2\varphi)d\varphi \,. \tag{25}$$

The other, developed by Hughes & De Leeuw (1965), considers a series of beamlets comprising the flow.[17] Both methods produce different expressions, with the same numeric results.

D. Multi-Channel micro-RPA Current Collection Theory

The directionality of the MCP allows for the valid assumption that the cylindrical channel effects and applied retarding potential can be treated independently. That is, all geometric flux limitation occurs within the microchannels. Upon entry into the RPA electrode series, the plasma is directional. Minimal flux limitation due to the geometry of the electrode series will occur. Similarly, since the MCP is spot-welded to the FE, the MCP is inherently grounded to the RPA housing. Therefore, minimal voltage sweeping will occur within the microchannels.

The resultant CCT requires the calculation of an MCP transmission fraction in similar fashion as developed in Partridge et al. (2003), as shown by

$$\chi_{\text{MCP}} = \frac{N_{cc}(S, D_{\text{MCP}})}{N_{cc}(S,\infty)} \tag{26}$$

where the numerator represents the flux exiting the Microchannel, and the denominator represents the flux entering an infinitely-thin orifice of the same diameter (entering flux).[11] The **current collection equation for an MC-µRPA** is then

$$I_{D\mu RPA} = \chi_{\text{MCP}} qAN_i = \chi_{\text{MCP}}\frac{qAn}{2\pi^{3/2}}\left[\frac{\exp(-\beta^2(v_{eff}-c_0)^2)}{\beta} + v_{dr}\sqrt{\pi}\{1-\text{erf}(\beta(v_{eff}-c_0))\}\right] \tag{27}$$

where A corresponds to the effective transparent area of the MCP.

E. Single-Channel micro-RPA Current Collection Theory

Without an MCP, cylindrical flux limitations and voltage sweeping both occur throughout the single-channel electrode series. Recall from Section B that the distribution of speeds for a Maxwellian drifting plasma with an applied potential will have the form

$$\dot{N}_s = \frac{n_s}{\beta\pi^{3/2}} \int_0^{\pi/2} \int_{Veff/\cos\theta}^{\infty} \int_0^{2\pi} \Xi^3 \cos\theta \exp(-(\Xi^2 + S^2 - 2\left|\vec{\Xi}\right|\left|\vec{S}\right|\cos\theta)) \sin\theta d\phi d\Xi d\theta \,. \tag{28}$$

Integration over Ξ must be performed first to incorporate the cylindrical channel flux limitation. Next, integration over θ must be performed from zero to some arbitrary angle ζ. Third, integration of ζ from zero to $\arctan(D\sqrt{1-Y^2})$, followed by a final integration over Y from zero to one. The number flux is reduced to include only the species traveling through the RPA without a wall collision, in accordance with the 100% wall absorption assumption. The result is the following:

$$N_{cc} = \frac{n_s}{\beta\pi^{3/2}} \int_0^1 \int_0^{\arctan\left(D\sqrt{1-Y^2}\right)} \int_0^{\zeta} \int_{Veff/\cos\theta}^{\infty} \Xi^3 \cos\theta \exp(-(\Xi^2 + S^2 - 2\left|\vec{\Xi}\right|\left|\vec{S}\right|\cos\theta)) \sin\theta d\Xi d\theta d\zeta dY \,. \tag{29}$$

Integration yields

$$N_{cc} = \frac{2nrl}{\sqrt{\pi}\beta} \int_0^1 \int_0^{\arctan\left(D\sqrt{1-Y^2}\right)} \frac{1}{\cos^2(\zeta)} \int_0^{\zeta} \tan(\phi) \exp\left(\frac{-V^2 - 2S^2\cos^2(\phi) + S^2\cos^4(\phi)}{\cos^2(\phi)}\right)$$
$$\left[\begin{array}{l} \cos^2(\phi)\exp(2VS + S^2 - S^2\cos^2(\phi)) \\ +S\cos^2(\phi)\exp(2VS + S^2 - S^2\cos^2(\phi)) \\ +V^2\exp(2VS + S^2 - S^2\cos^2(\phi)) \\ +S^2\cos^4(\phi)\exp(2VS + S^2 - S^2\cos^2(\phi)) \\ +\frac{3}{2}\sqrt{\pi}S\cos^3(\phi)\exp\left(\frac{V^2 + S^2\cos^2(\phi)}{\cos^2(\phi)}\right) \\ +S^3\sqrt{\pi}\cos^5(\phi)\exp\left(\frac{V^2 + S^2\cos^2(\phi)}{\cos^2(\phi)}\right) \\ -S^3\sqrt{\pi}\cos^5(\phi)\exp\left(\frac{V^2 + S^2\cos^2(\phi)}{\cos^2(\phi)}\right) erf\left(\frac{V - S\cos^2(\phi)}{\cos(\phi)}\right) \\ -\frac{3}{2}\sqrt{\pi}S\cos^3(\phi)\exp\left(\frac{V^2 + S^2\cos^2(\phi)}{\cos^2(\phi)}\right) erf\left(\frac{V - S\cos^2(\phi)}{\cos(\phi)}\right) \end{array}\right] d\phi d\zeta dY \tag{30}$$

which is defined as the **SC-μRPA current collection equation**. As in the case of a drifting Maxwellian plasma with an applied potential as developed in spherical coordinates, the error function of a cosine requires numeric integration. Validation of the SC-μRPA current collection equation is done by comparison with the previously derived extreme cases: 1. The case of a relatively thin orifice at various potentials as shown in Figure 7. 2. The case of an unbiased or unsegmented channel of various diameter to length ratios, as shown in Figure 8. Ion parameters used were: Carbon, $n = 5.5\text{x}10^{16} m^{-3}$, $S = 1.187$, $T = 10eV$, and $d = 200\mu m$.

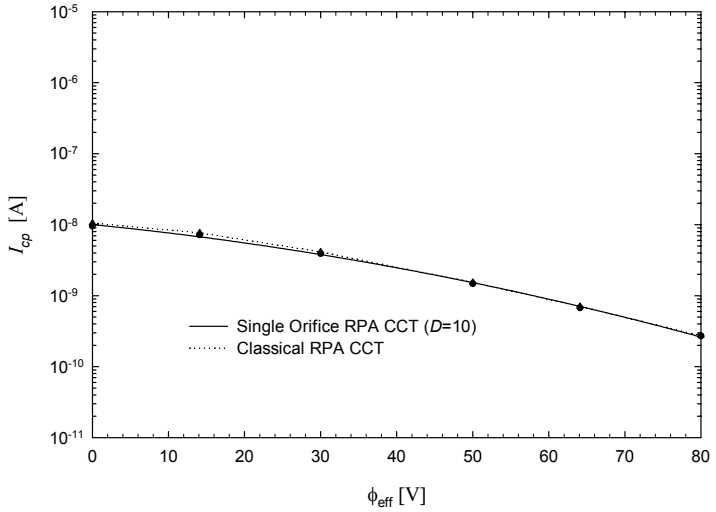

Figure 7. SC-μRPA CCT validation: Thin orifice.

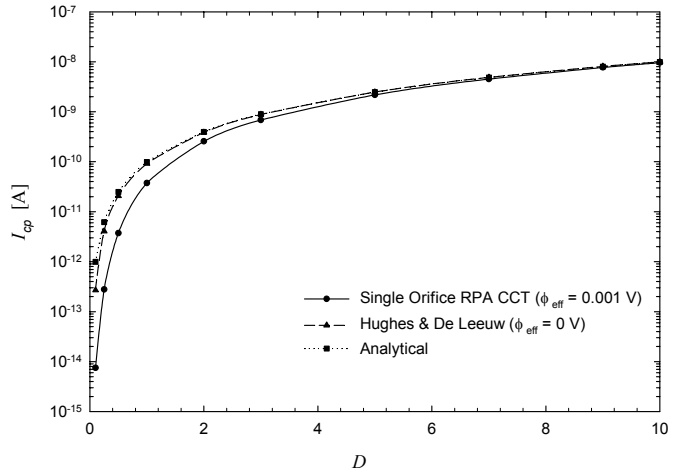

Figure 8. SC-μRPA CCT validation: Unsegmented channel.

There is some error at low diameter to length ratios, but the SC-μRPA CCT shows overall agreement in both cases.

III. Numerical Evaluation and Validation

A. Numerical Integrator

Math solvers such as Maple[15], Mathematica[16], and Mathcad[18] were unable to numerically integrate the SC-μRPA current collection equation for relatively low plasma temperatures (less than 10 eV), particularly due to the functionally dependent upper bounds. A triple numeric integrator program was subsequently developed in FORTRAN to accurately calculate the expected collector plate current for any given set of plasma parameters and SC-μRPA dimensions.

Since the functionally dependent upper bounds of the current collection equation required that the integration be performed serially from the innermost integral to the outermost integral, rather than separately, the program incorporated a series of nested Simpson's rule approximation subroutines. For every one subinterval calculation for the outermost integral's approximation, an entire Simpson's rule approximation must be performed for the middle integral. Likewise, performing each subdivision calculation of the middle integral's approximation requires an

entire Simpson's rule approximation for the innermost integral. For example, a subinterval resolution of 100 x 100 x 100 for the outermost, middle, and innermost integrals respectively will require 10,000 Simpson's rule subinterval calculations for the middle integral, which will in turn require 1,000,000 subinterval calculations for the innermost integral. Since the innermost integral contains approximately more than 150 operations, with both the middle and outermost integral containing roughly five operations each, the result will involve more than 150,050,500 operations total.

B. Validation and Error

To ensure validity of the triple numeric integrator concept, test cases of various triple integrals with functionally dependent upper bounds were tested at various resolutions. For the current collection equation, it was found that there was less than a 2% error with subdivision resolution of 10,000 x 10,000 x 1,000 for the outer, middle, and inner integral respectively. Since the inherent accuracy of the Simpson method is based on the fourth derivative of the integrated function, increasing the inner integral subintervals from 1,000 to 10,000 would only slightly increase accuracy (ranging from a 0.45% to 0.70% increase for Carbon plasma) at the cost of significant computational time.

To check the validity of the triple numeric integrator program as it applies to the SC-μRPA CCT, comparison of its data to that of existing complimentary data (greater than $10eV$) from the math solvers was required. I-V curve comparisons for the test RPA geometry of $D = 0.095$ at various effective potentials are shown in Figure 9. The voltage sweep was performed for Carbon at ion speed ratios of $S = 0.1,\ 1.0, \text{and}\ 5.0$, with $n = 1\text{x}10^{15} m^{-3}$. $S = 1.0$ is shown, containing the largest error of 1.3% at $\phi = 80V$. Subinterval resolution was 10,000 x 10,000 x 1,000 for the outermost, middle, and innermost integral respectively.

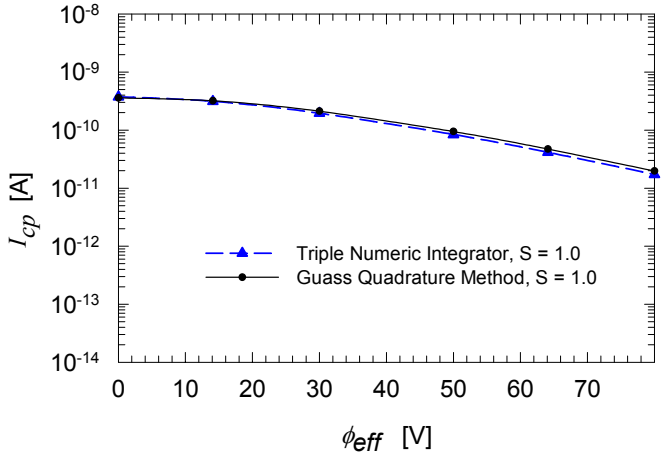

Figure 9. Validation of the triple numeric integrator program.

The error associated with the Simpson's rule approximation can be calculated for each integral as a function of the subinterval resolution, the integral bounds, and the fourth derivative of the integrand. For a single integral with finite bounds, the Simpson's rule approximation error is given as

$$\left|ES_n\right| \le \frac{M_4 (b-a)^5}{180 n^4} \tag{31}$$

where M_4 is the maximum absolute value of the fourth derivative of the integrand $f(x)$, provided that n is even and $f(x)$ is continuous on the interval $[a,b]$.[19]

For a triple integral with functionally dependent upper bounds in the innermost and middle integrals, kept in general form as

$$\int_a^b f_1(x) \int_c^{g_1(x)} f_2(y) \int_d^{g_2(y)} f_3(z) dz dy dx\,, \tag{32}$$

the error becomes

$$\left|ES_{n,Total}\right| \le \frac{M_{4,Outer}(b-a)^5}{180n_{Outer}^4} + \sum_{i=1}^{n_{Outer}} \left(\frac{M_{4,Middle}(g_1(i*\Delta y)-c)}{180n_{Middle}^4} + \sum_{j=1}^{n_{Middle}} \frac{M_{4,Inner}(g_2(j*\Delta z)-d)}{180n_{Inner}^4} \right) \tag{33}$$

where subscripts $Outer$, $Middle$, and $Inner$ correspond to the Outermost, Middle, and Innermost integral respectively.

For the specific case of the current collection equation:

$$\begin{aligned} &a = c = d = 0 \\ &b = 1 \\ &g_{1,Max} = \arctan(D) \\ &g_{2,Max} = \arctan(D) \\ &f_1^4 = 0 \\ &f_2^4 = 16\sec^2(\zeta) + \\ &\quad 88\sec^4(\zeta)\tan^2(\zeta) + \\ &\quad 16\sec^2(\zeta)\tan^4(\zeta) \end{aligned} \tag{34}$$

and f_3^4 is approximately 2,500 terms in length. Exact values of f_3^4 are calculated in Mathematica[16] for specific cases. $M_{4,Middle} = 17.25$ for the test geometry of $D = 0.095$. $M_{4,Inner} \approx 1.06\text{x}10^6$, occurring at low effective retarding potentials and $S = 5.0$. For the test geometry, the total error of the triple numeric integration becomes

$$\left|ES_{n,Total}\right| \le \frac{2nrl}{\sqrt{\pi}\beta} \left(9.104\text{x}10^{-3} \frac{n_{Outer}}{n_{Middle}^4} + 5.278\text{x}10^{-4} M_{4,Inner} \frac{n_{Outer} n_{Middle}}{n_{Inner}^4} \right). \tag{35}$$

Error bars generated from (35) are displayed on Figure 13 and Figure 14 (See Appendix). A majority of the error bars are less than 5%, which do not appear on a logarithmic scale. The maximum error is less than 60%, occurring at zero ion retarding potential and relatively high ion speed ratios.

IV. Determination of Plasma Parameters

Determining macroscopic plasma parameters from experimentally obtained I-V curve data is essentially the inverse problem of developing a valid current collection model. Nonlinear least squares regression of the classical RPA current collection theory has been implemented as a means to extract plasma parameters from experimental data for traditional gridded RPAs. Specifically, ion number density, ion velocity, ion temperature, and species concentrations can be calculated for a traditional gridded RPA through the summation of individual species distribution functions.[20,21] Similar analysis can be applied towards data obtained from an MC-μRPA. The MCP transmission fraction simply appears as a constant in the derivatives matrix, and the least squares fit is performed.

However, such analysis cannot be applied to the single-channel micro-RPA current collection theory, since the process is based on numeric integration. It is necessary to perform an iterative method of comparing the sample I-V data with that of the triple numeric integrator. This Ion Parameter Extraction Method (IPEM) has been implemented using MATLAB.[22] The IPEM schematic, including specific fuzzy logic rules, are demonstrated in Figure 12.

First, the IPEM program imports the I-V curve sample (experimental) data and polyfits the available data points to produce an averaged curve with data points at desired effective voltage values. An example of the polyfit is shown in Figure 10.

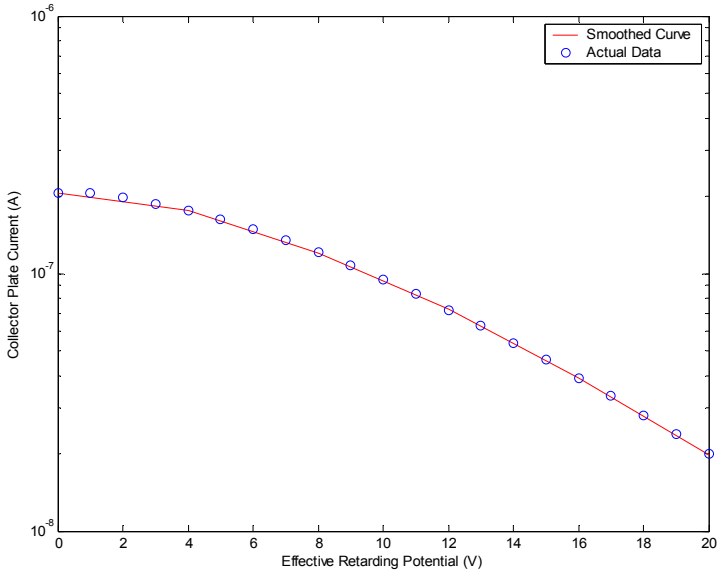

Figure 10. I-V sample data and polyfit smoothed curve.

Assuming a known RPA geometry and a single ion species of known mass, the triple numeric integrator program is run at initial guess values for ion density, temperature, and speed ratio. The resultant TNI-generated I-V curve is compared to that of the polyfit sample data. The difference and slope at each data point (every 5V from 0V to 20V) is calculated, as well as the total error. IPEM is limited to the assumption that the RPA channel is at a constant effective retarding potential, causing data points at potentials greater than ~25 V to be ignored. This allows for close scrutiny of I-V curve behavior at relatively low ion temperatures (less than 1.0 eV), which are sensitive to effective retarding potentials higher than 25 V.

Fuzzy logic was employed to increase the accuracy and minimize computational time throughout this process. Using the fuzzy logic toolbox in MATLAB[22], a set of four rules was developed to determine parameter modifications for the next iteration. For example, the first IPEM rule states that if the current calculated by the triple numeric integrator is *less than* that of the sample data at an effective potential of 0V, the number density value to be used for the next iteration, n_{TNI}, will be *increased* by $1\text{x}10^{(O(n_{TNI})-1)}$. Once the total error is constant (fluctuating between two values at every other iteration) the iteration stops, ion drift velocity based on ion speed ratio and temperature is calculated, and all final parameters (including total error) are output. IPEM convergence has been validated using a sample I-V curve of known ion parameters, such that the end result outputs the aforementioned parameters within 5% error. Convergence behavior of the IPEM program is shown in Figure 11.

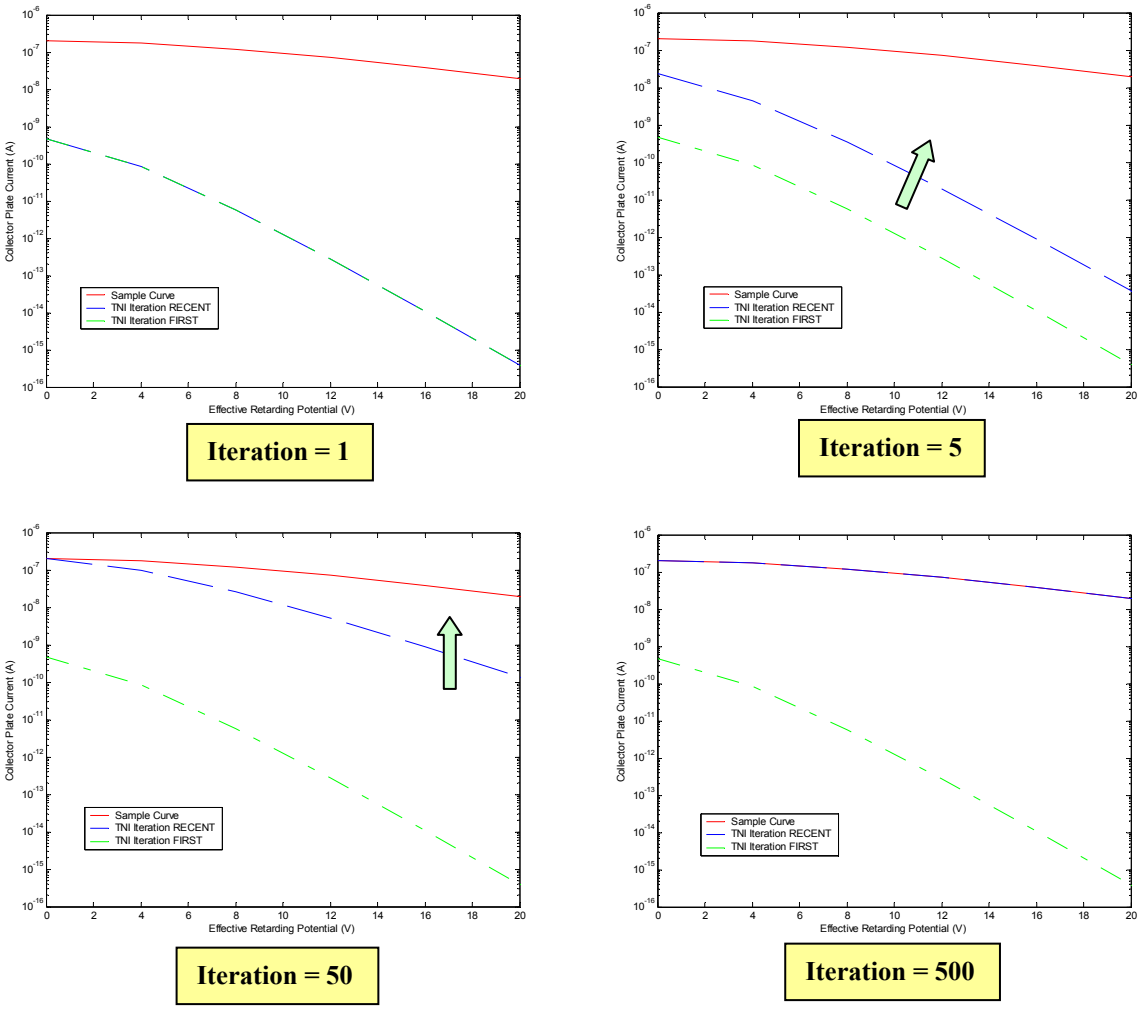

Figure 11. IPEM Convergence: Sample I-V curve and TNI-generated I-V curves at various iterations.

Further reduction of the error can be achieved by optimizing the fuzzy logic rules to decrease the step size for each modification of the guess values, but is not necessary. A majority of the error exists in the polyfit of the initial sample data, which is the function of the number of degrees specified for the polyfit function, as well as the perturbation of the I-V curve sample data from a TNI generated curve. The error for each TNI generated curve is then equal to the sum of the TNI error at each data point, as derived in the previous section.

V. Results and Discussion

Data obtained from the triple numeric integrator program for a broad range of Carbon and Xenon plasmas are contained in Figure 13 and Figure 14, respectively. All plasmas are assumed to consist of a single species of singly-charged monatomic positive ions, with the low energy electrons assumed to have been entirely repelled by the ERE and SESE. The test RPA geometry used throughout has a diameter $d = 200\mu m$ and length $l = 2100\mu m$, resulting in a diameter to length ratio of $D \approx 0.095$ with no MCP. I-V curves were generated for each plasma at three different number densities ($n = 1\text{x}10^{15}\, m^{-3}$, $1\text{x}10^{18}\, m^{-3}$, $1\text{x}10^{21} m^{-3}$), three different ion temperatures ($T = 0.1eV$, $1.0eV$, $10.0eV$), and three different ion speed ratios ($S = 0.1$, 1.0, 5.0). Data points were calculated at effective ion retarding potentials of $\phi = 0.0V$, $14.1V$, $30.0V$, $50.0V$, $64.1V$, and $80V$.

The ions are exceedingly susceptible to any retarding potential at relatively low temperatures, regardless of drift velocity. At higher temperatures, high ion speed ratios will tend to eliminate the effects of the retarding potential. The magnitudes of the predicted current values at relatively low ion retarding potentials (less than $20V$) are of particular interest. Magnitudes at relatively high temperatures range from microamps to nanoamps, which is to be expected during experimental implementation of the test RPA. It is clear that the triple numeric integration scheme and ion parameter extraction method are valid.

VI. Conclusion

RPA entrance areas are subjected to the $2\lambda_D$ constraint in order to avoid space charge limitations. For relatively high-density plasmas, this constraint will either oblige small RPA dimensions or necessitate filtration of the incident plasma through an entrance slit or low-transparency mesh. In either case, classical RPA current collection theory no longer applies.

This paper presented the development and validation of a robust current collection theory capable of accurately portraying a broad range of plasmas for both the SC-μRPA and the MC-μRPA. Since the triple numeric integrator program used to calculate each data point employed a series of nested Simpson's rule approximation subroutines, the accuracy of the SC-μRPA CCT is limited to all three subinterval resolutions as well as the constant effective retarding potential assumption. The MC-μRPA CCT is limited to the accuracy of the assumption that the cylindrical channel flux limitations occur entirely within the MCP. I-V curve data is presented for two monatomic plasmas at various densities, temperatures, and speed ratios. The reverse process was also fully resolved: extraction of the aforementioned parameters from sample I-V curve data using an iterative method employing the TNI program where nonlinear regression was no longer valid.

Appendix – IPEM Schematic and TNI-Generated I-V Curves

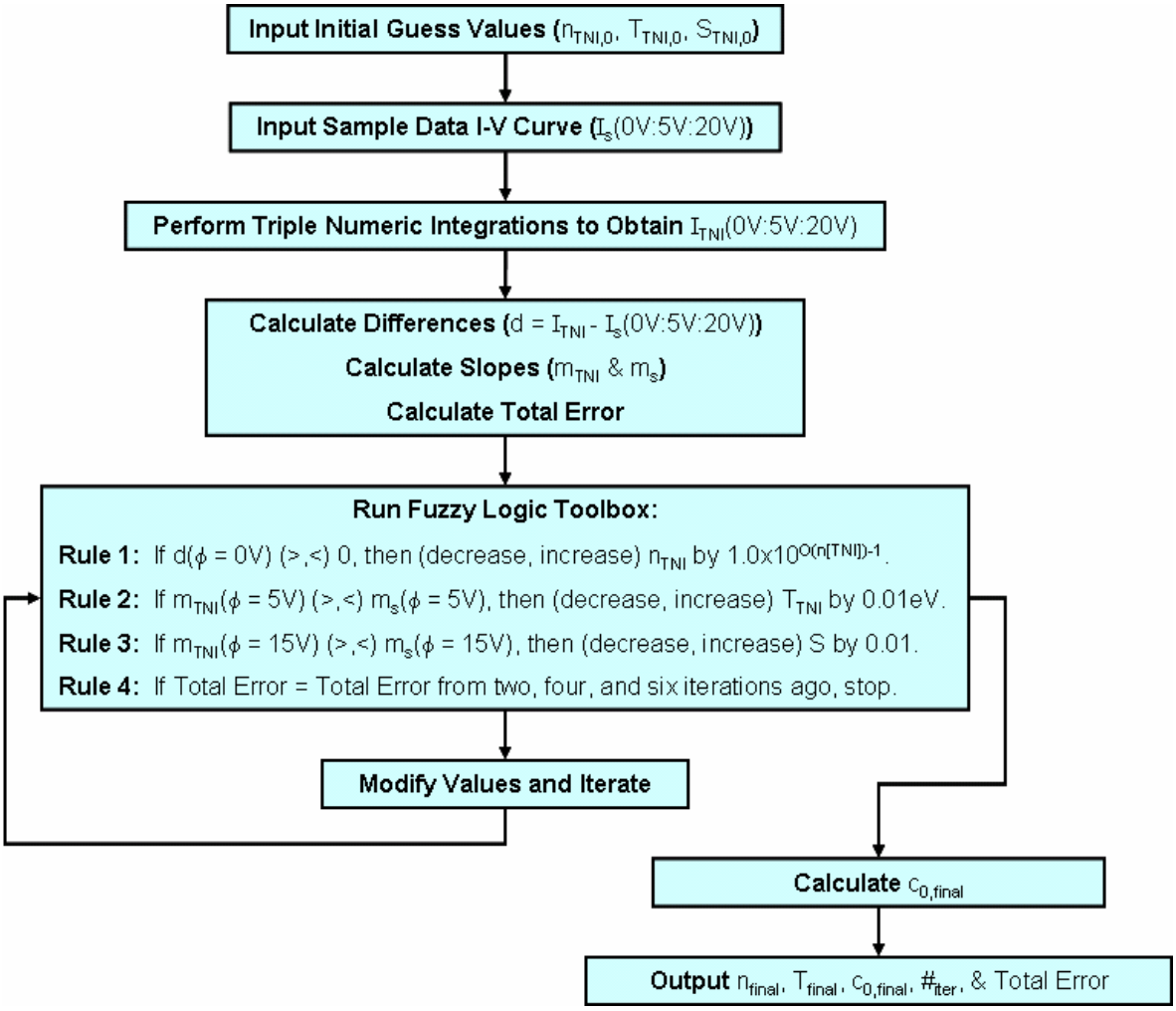

Figure 12. Ion Parameter Extraction Method (Assumes D and m known, single species).

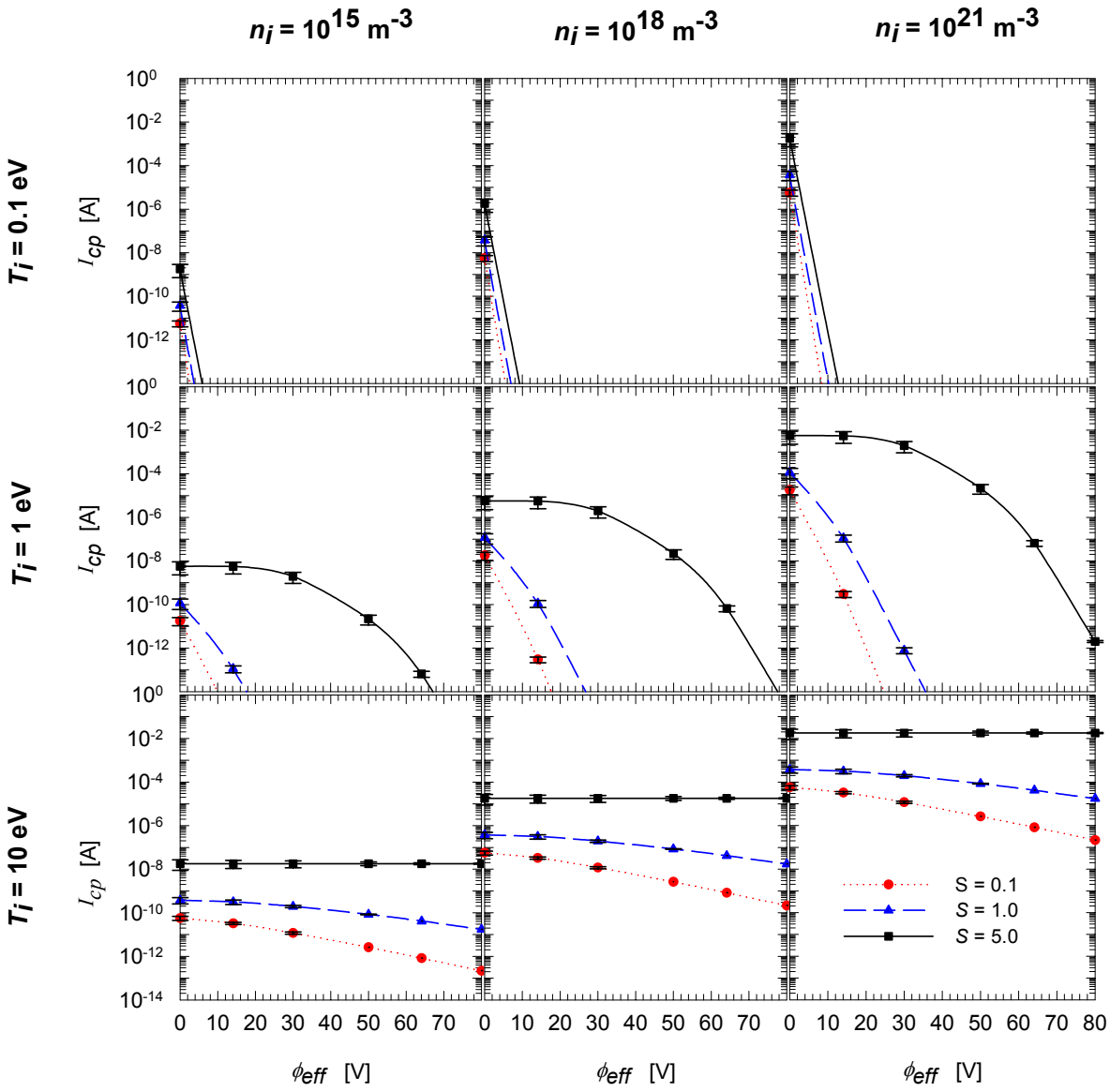

Figure 13. SC-μRPA CCT results for Carbon.

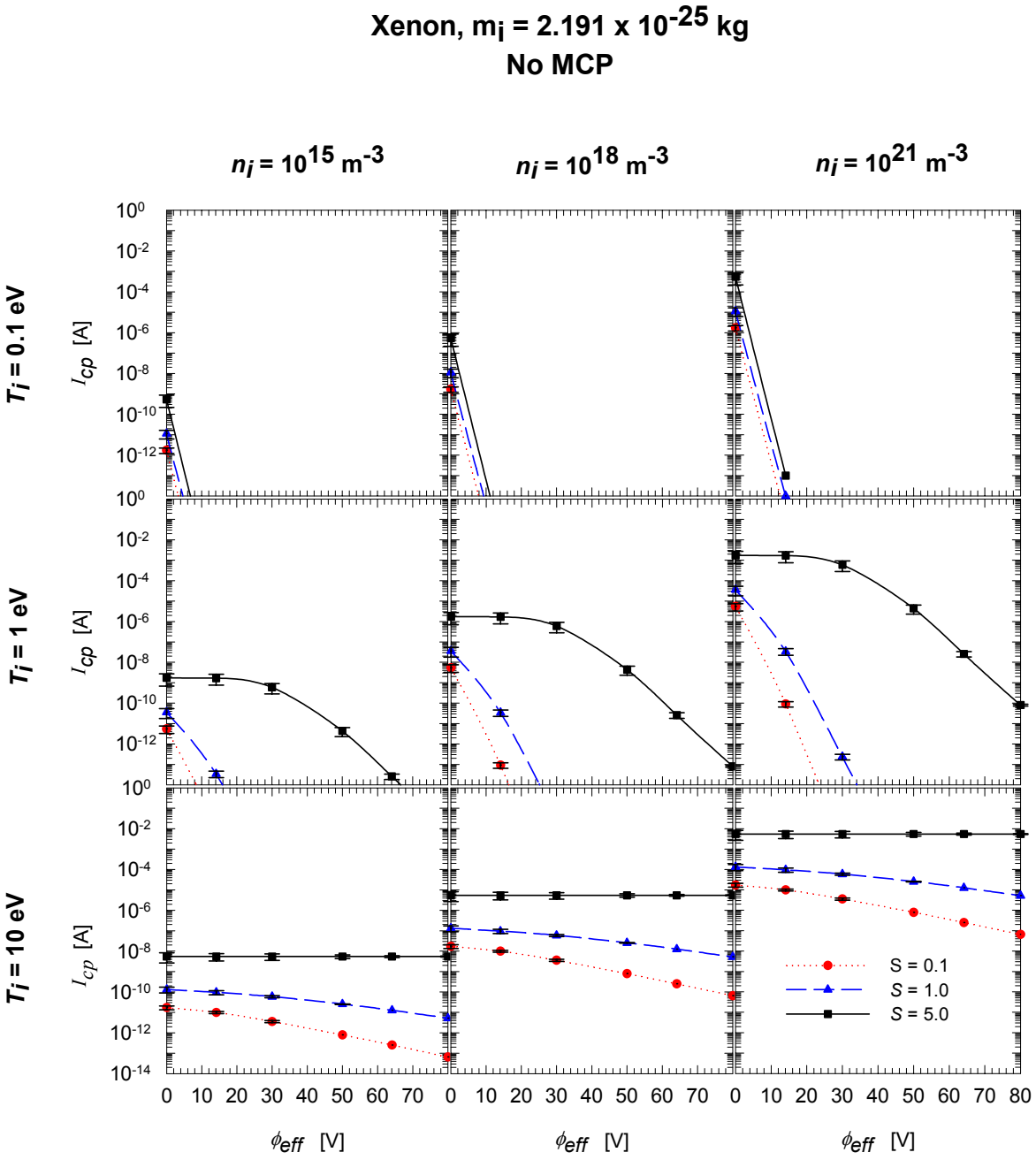

Figure 14. SC-µRPA CCT results for Xenon.

Acknowledgments

This research was funded partly by the Massachusetts Space Grant Consortium as well as NASA NAG3-2405. The authors would also like to acknowledge Professor John J. Blandino and Dr. David L. Cooke for useful discussions relevant to the design of the SC-μRPA and MC-μRPA.

References

[1] Partridge, J., and Gatsonis, N.A., "Validation of a Directional Micro-Retarding Potential Analyzer for High-Density Plumes," AIAA-2005-4048, July, 2005.
[2] Huddlestone, R.H. and Leonard, S.L., *Plasma Diagnostic Techniques*, Academic Press, Inc., 1965.
[3] Kelley, M.C., "The Earth's Ionosphere: Plasma Physics and Electrodynamics," Academic Press, Inc., 1989.
[4] King, L.B. and Gallimore, A.D., "Gridded Retarding Pressure Sensor for Ion and Neutral Particle Flux in Flowing Plasmas", AIAA-96-2983, July 1996.
[5] Giffin, G.B., "Analysis of the Ion Current Collection in the Plasma Wake During the Charging Hazards and Wake Studies (CHAWS) Experiment," Master of Science Thesis, Aeronautics and Astronautics Department, Massachusetts Institute of Technology, 1996.
[6] Raitt, W.J. and Thompson, D.C., "Thermal Plasma Measurements in Space Using Direct Measurements of Derivatives of Probe Current-Voltage Characteristics," Measurement Techniques in Space Plasmas: Particles, American Geophysical Union, c1998.
[7] Marrese, C.M., Majumdar, N., Haas, J., Williams, G., King, L.B., and Gallimore, A.D., "Development of a Single-orifice Retarding Potential Analyzer for Hall Thruster Plume Characterization," IEPC-97-066, *25th International Electric Propulsion Conference*, August 1997, Cleveland, OH.
[8] Green, T.S., "Space Charge Effects in Plasma Particle Analyzers," *Plasma Physics*, Vol.12, pp. 877-883, 1970.
[9] Hora, H., *Plasmas at High Temperature and Density*, Lecture Notes in Physics, Springer-Verlag, 1991.
[10] Hutchinson, I.H., *Principles of Plasma Diagnostics*, Cambridge University Press, 1987.
[11] Partridge, J., Gatsonis, N.A., and Pencil, E.J., "Preliminary Design and Analysis of a Directional Micro-Retarding Potential Analyzer for High-density Plumes," AIAA-2003-5172, July, 2003.
[12] Chapman, S. and Cowling, T.G., *The Mathematical Theory of Non-Uniform Gases*, 3rd Edition, Cambridge University Press, 1970.
[13] Bird, G.A., *Molecular Gas Dynamics and the Direct Simulation of Gas Flows*, Clarendon Press, 1994.
[14] Patterson., G.N., *Introduction to the Kinetic Theory of Gas Flows*, University of Toronto Press, 1971.
[15] Maple, Ver 9.01, Maplesoft, a division of Waterloo, Inc., 2003.
[16] Mathematica, Ver. 5.0.0.0, Wolfram Research Inc., 2003.
[17] Hughes, P.C. and de Leeuw, J.H., "Theory for the Free Molecule Impact Probe at an Angle of Attack," *Rarefied Gas Dynamics*, Vol.1, p. 653, 1965.
[18] Mathcad 2001i Professional, MathSoft Engineering & Education, Inc., 2001.
[19] Edwards Jr., C.H. and Penney, D.E., *Calculus and Analytical Geometry*, 3rd Edition, Prentice-Hall, Inc. c1982.
[20] Burton, T.A., Parker, K., and Shumlak, U., "Exhaust Plume characterization of a Mini-PPT Using a Time-of-Flight/Gridded Energy Analyzer," AIAA-2002-4122, *38th Joint Propulsion Conference*, July 7-10, 2002, Indianapolis, IN.
[21] Shumlak, U., Burton, T.A., and Parker, K.M., "Mass Characterization Measurements of a Mini-PPT Exhaust Plasma," AIAA-2003-5169.
[22] MATLAB, Ver. 6.5.1.199709 Release 13, The MathWorks, Inc., 2003.